

# Elasticity, Stability and Ideal Strength of $\beta$ -SiC in plane-wave-based *ab initio* calculations

Weixue Li and Tzuchiang Wang

*LNM, Institute of Mechanics, Chinese Academy of Sciences, Beijing, 100080,  
China*

## Abstract

On the basis of the pseudopotential plane-wave(PP-PW) method and the local-density-functional theory(LDFT), this paper studies energetics, stress-strain relation, stability and ideal strength of  $\beta$ -SiC under various loading modes, where uniform uniaxial extension and tension, biaxial proportional extension are considered along directions  $[001]$  and  $[111]$ . The lattice constant, elastic constants and moduli of equilibrium state are calculated, and the results agree well with the experimental data. As the four Si-C bonds along directions  $[111]$ ,  $[\bar{1}11]$ ,  $[11\bar{1}]$  and  $[1\bar{1}\bar{1}]$  are not the same under the loading along  $[111]$ , internal relaxation and the corresponding internal displacements must be considered. We find that, at the beginning of loading, the effect of internal displacement through shuffle and glide plane diminishes the difference among the four Si-C bonds length, but will increase the difference at the subsequent loading, which will result in a crack nucleated on  $\{111\}$  shuffle plane and a subsequently cleavage fracture. Thus the corresponding theoretical strength is 50.8 GPa, which agrees well with the recent experiment value, 53.4 GPa. However, with the loading along  $[001]$ , internal relaxation is not important for tetragonal symmetry. Elastic constants during the uniaxial tension along  $[001]$  are calculated. Based on the stability analysis with stiffness coefficients, we find that the spinodal and Born instabilities are triggered almost at the

same strain, which agrees with the previous molecular dynamics simulation. During biaxial proportional extension, stress and strength vary proportionally with the biaxial loading ratio at the same longitudinal strain.

## I. INTRODUCTION

Investigation of stability and ideal strength of materials is always an attractive issue <sup>[1]- [9]</sup> due to the following facts: (1). Stability of materials is very important in elasticity theory, which is related with structural responses in solids, ranging from ploy-morphism, amorphization, and melting to fracture. <sup>[10]- [13]</sup> (2). The ideal strength of a perfect crystal represents an upper bound to the actual strength of crystalline materials; (3) The technology makes it possible to manufacture finer and finer filament, whose strength will approach the theoretical limit. However, even for the best whisker materials. <sup>[14], [15]</sup>, the realistic strength is still far below the predicted theoretical values.

Recent developments of experimental technology see new opportunities of producing very fine nanorods (NRs) and nanotubes (NTs) <sup>[16]- [20]</sup>, and the possibility of measuring their elasticity constants, strength and toughness, <sup>[21], [22]</sup>. The typical measured diameter of NRs is 20-30 nanometer, which can be considered free of any defects and with the ideal strength. Wong *et al.* <sup>[22]</sup> measured the Young's modulus and the bending strength of silicon carbide (SiC) NRs in a recent experiment. It is worth mentioning that micrometer-scale SiC whisker is widely used to strengthen composite materials. Thus, it is necessary to have a clear understanding of the stiffness, stress-strain relation, stability and strength of these nano sized NRs from the experimental view as well as from the theoretical point of view.

As is well known, people are used to study the ideal strength of materials with various models and empirical potentials. Polanyi <sup>[23]</sup> and Orowan <sup>[24]</sup> used a model in terms of surface energy, interplanar space and an appropriate Young's modulus to investigate the ideal strength. Frenkel <sup>[1]</sup> estimated ideal shear strength  $\tau_{max}$  of a solid subjected to deformation of a simple shear mode. However, oversimplified functions of stress-strain were adopted in those methods and the functional forms for different materials were somehow arbitrary. On the basis of stability criteria, Milstein <sup>[3], [4], [5]</sup> investigated theoretical strength of bcc Fe, fcc Ni and Cu with the Morse potential. The ideal strength is identified with the loss or exchange of stability. This method helps greatly the investigation of strength and reveals

a variety of interesting and surprising behaviors of materials <sup>[25], [26], [27], [28]</sup>; however, the interatomic potential they used and obtained by fitting properties of equilibrium state is inappropriate to be used for the investigation of the stability and strength of materials, which are essentially of far from being in the equilibrium state. On the other hand, the density functional theory(DFT) <sup>[29]</sup> , with only the input of atomic position and charge number , can be used to determine many structural and dynamic properties of materials under various conditions, including those, which are far from being in the equilibrium state.

Through a series of comprehensive theoretical and computational studies, Hill and Milstein <sup>[31], [32], [33]</sup> have shown that positive definiteness of internal energy is coordinate dependent and the stability domain depends on the choices of strain measures; while Born criteria <sup>[30]</sup> are valid only under the zero load. Based on this idea, Wang *et al.* <sup>[11], [12]</sup> analyzed the onset of instabilities in homogeneous lattice under critical loading and showed that response of the lattice is no longer a purely intrinsic property of materials, and depends on the applied load. Starting with these theories, Li and Wang <sup>[34]</sup> have recently analyzed the stability and branching of Aluminium under various loading modes according to the first principle calculations.

Heine and co-workers <sup>[35], [36]</sup> gave a very extensive set of first principle pseudopotential calculations on the ploy-types in SiC. However, they gave only the bulk modulus. Lambrecht *et al.* <sup>[37]</sup> made a detailed investigation on the elastic constants, modulus of  $\beta$ -SiC with the full-potential linear-muffin-tin-orbital (FP-LMTO) method. In their investigations, the strength of  $\beta$ -SiC was obtained approximately by Orowan formula. The structural properties of  $\beta$ -SiC(ploy-type 3C) had been also investigated by the various semi-empirical models, e.g. , semi-empirical force model <sup>[38]</sup>, semi-empirical interatomic potential <sup>[39], [40]</sup> and tight binding approximation <sup>[41], [42]</sup>. Modifying the Tersoff potential <sup>[39]</sup>, Tang and Yip <sup>[43]</sup> investigated the lattice instability in  $\beta$ -SiC and simulated the process of brittle fracture under hydrostatic tension based on the Hill and Milstein stability theory. The instability mode is the spinodal instability, and decohesion occurs as spontaneous nucleation of cracking on the

$\{111\}$  shuffle planes.

In the present paper, we study the energetics, the elastic constants, the stress-strain relation, stability and the ideal strength of  $\beta$ -SiC with the density functional theory. We consider several loading modes, uniaxial extension and uniaxial tension along  $[001]$  and  $[111]$  directions, and biaxial proportional extension along  $[001]$  and  $[010]$ . The deformation is homogeneous and elastic, and the strain can be large. The stress-strain relations are calculated, and the ideal strength is obtained according to the stability criteria. Owing to the unequivalence of the four Si-C bonds under the loading along  $[111]$ , the internal relaxation must be considered and the internal displacements be calculated. With the internal displacements, we discuss the effect of the relaxation and failure modes. The stability theory of Hill and Milstein <sup>[31], [32], [33]</sup> and Wang <sup>[12]</sup> are used to discuss branching and the strength of  $\beta$ -SiC under the loading along  $[001]$ .

The present paper is organized as follows. The calculation model is presented in Sec. II, where we show the formulation of stress, elastic stiffness coefficients and stability criteria, especially the three loading modes with the selection of supercell and the numerical precision illustrated at the end of this Section. The benchmark, including equilibrium properties and elastic constants, are given in Sec. III. The loading along  $[111]$  direction is presented in Sec. IV, and biaxial proportional extension is investigated in Sec. V. In Sec. VI, we discuss uniaxial extension and tension along  $[001]$  direction. Summary and conclusion are given in Sec. VII.

## II. FORMULATION

Consider an unstressed and unstrained configuration, denoted as  $\mathbf{X}_0$ . It undergoes homogeneous deformation under a uniform applied force, and changes from  $\mathbf{X}_0$  to  $\mathbf{X} = \mathbf{J}\mathbf{X}_0$ , where  $\mathbf{J}$  is the deformation gradient or the Jacobian matrix. The associated Lagrangian strain tensor  $\mathbf{E}$  is:

$$\mathbf{E} = \frac{1}{2}(\mathbf{J}^T \mathbf{J} - \mathbf{I}) \quad (1)$$

where  $T$  is transpose. The physical strain is:

$$\mathbf{e} = \mathbf{J} - \mathbf{I} \quad (2)$$

For the present deformation, the internal energy  $U$  is a rotational invariant and therefore only a function of  $\mathbf{E}$ . The second Piola-Kirchhoff stress tensor  $\mathbf{T}$  <sup>[44]</sup> is defined as:

$$T_{ij} = \frac{1}{V_0} \frac{\partial U}{\partial E_{ij}} \quad (3)$$

It is related to Cauchy stress, *i.e.* the true stress  $\sigma_{kl}$  by the following equation:

$$T_{ij} = \mathbf{det}|\mathbf{J}| J_{ik}^{-1} J_{jl}^{-1} \sigma_{kl} \quad (4)$$

where  $\mathbf{det}|\mathbf{J}|$  is the ratio  $V/V_0$ . With the Cauchy stress, the applied force can be obtained by multiplying the current transverse area.

At strained state  $\mathbf{X}$ , the elastic constants are determined through the following equation:

$$C_{ijkl}(X) = \frac{1}{V(X)} \left( \frac{\partial^2 U}{\partial E'_{ij} \partial E'_{kl}} \right)_{E'=0} \quad (5)$$

where  $\mathbf{E}'$  is Lagrangian strain around the state  $X$ . These elastic constants are rotational invariant and symmetric with interchange of indices  $i \leftrightarrow j$ ,  $k \leftrightarrow l$  and  $(ij) \leftrightarrow (kl)$ , which are often expressed in the condensed Voigt notation.

To analyze the stability, the elastic stiffness coefficient  $\mathbf{B}$  <sup>[12]</sup> is introduced as follows:

$$B_{ijkl} = C_{ijkl} + \frac{1}{2} (\delta_{ik} \sigma_{jl} + \delta_{jk} \sigma_{il} + \delta_{il} \sigma_{jk} + \delta_{jl} \sigma_{ik} - 2\delta_{kl} \sigma_{ij}) \quad (6)$$

From this definition, we can see that  $\mathbf{B}$  does not possess  $(ij) \longleftrightarrow (kl)$  symmetry generally.

The system may be unstable when

$$\mathbf{det}|\mathbf{B}| = 0 \quad (7)$$

for the first time.

The following loading modes are considered:

(i) Uniaxial Extension.

$$e_{ij} = e\delta_{i3}\delta_{j3}, \quad i, j = 1, 2, 3 \quad (8)$$

(ii) Uniaxial Tension.

$$\sigma_{ij} = \sigma\delta_{i3}\delta_{j3}, \quad i, j = 1, 2, 3 \quad (9)$$

For a given longitudinal strain, let the transverse lattice contract or dilate to make the total energy approach minimum, which corresponds zero stress(traction) on lateral faces. For crystal symmetry, the transverse contraction is the same at two perpendicular transverse directions, so

$$e_{11} = e_{22} = -\lambda e_{33} \quad (10)$$

(iii) Biaxial Proportional Extension

$$e_{22} = \alpha e_{33} \neq 0 \quad e_{ij} = 0 \quad \text{others} \quad (11)$$

The total energy calculations are carried out with *ab initio* pseudopotential plane-wave program package Fhi96md.<sup>[45]</sup> By means of the mechanism of Hamman<sup>[46]</sup> and Troullier<sup>[47]</sup>, the soft first principle pseudopotential<sup>[48], [49]</sup> is generated, where the local density approximation(LDA) with the exchange and correlation energy functional developed by Perdew and Zunger<sup>[50]</sup> is used. Two supercells are designed in our calculations: one is the 8-atom supercell for the equilibrium properties, the loading along [001] and biaxial extension along [010] and [001]. The other one is the 6-atom supercell for the loading along [111]; in this case, the stacking consequence is Si-C-Si-C-Si-C. There exist two types of {111} plane, between Si and C atoms, corresponding to the well known glide and shuffle planes. The glide plane cuts three Si-C bonds out of four, and the shuffle plane cuts the remaining Si-C bond. For numerical differential feature of stress and elastic constants, the precision must be considered carefully. The size of carbon atom is so small that a high cut-off energy is required. Our test shows that  $E_{cut} = 80Ry$  has also given excellent results.. The k-space mesh is  $6 \times 6 \times 6$  for the 8-atom supercell and  $8 \times 8 \times 4$  for the 6-atom supercell in order to keep same precision.

### III. EQUILIBRIUM PROPERTIES

As the benchmark, we have calculated the lattice constant, elastic constants and moduli of  $\beta$ -SiC of equilibrium. For symmetry of  $\beta$ -SiC (zincblende structure), there exist three independent elastic constants, *i.e.*  $C_{11}$ ,  $C_{12}$ ,  $C_{44}$ . The total energy of  $\beta$ -SiC is calculated under the applied hydrostatic, uniaxial deformation, and trigonal strain. Owing to the lattice feature of zincblende structure, which includes two fcc lattices with a relative displacement along [111], the symmetry of center inversion is lost. Four Si-C bonds along directions [111],  $[\bar{1}\bar{1}1]$ ,  $[11\bar{1}]$  and  $[\bar{1}11]$  are not equivalent under the case of trigonal strain. The internal atomic position must be fully relaxed, and the internal displacement<sup>[51]</sup>, which refers to the relative displacement of two sublattices beside the displacement from the macroscopic strain, will take place. Our results are presented in Table I. From this table, we find, our results agree well with the experimental data and the previous first principle and semi-empirical calculations. The value of  $C_{44}$  without relaxation, 270 GPa, is already in good agreement with the experimental data and better than other theoretical calculations. The relaxed value, 254 GPa, is almost the same as the experiment value. Value of the anisotropy  $\mathbf{A}$  is also satisfactory.

Based on the representation surface<sup>[52]</sup>, the moduli along a certain direction can be obtained. The Young' modulus along directions [111] and [001] are 554 GPa and 338 GPa, respectively. Lambrecht *et al.*<sup>[37]</sup> obtained 603 GPa and 362 GPa. Petrovic *et al.*<sup>[15]</sup> measured Young's modulus of  $\beta$ -SiC whisker, with an averaged value of 578 GPa with  $\pm 10\%$  scattering. Applying the equation of the cantilever beam, Wong *et. al.*<sup>[22]</sup> measured Young's modulus of [111]-oriented SiC nanorod, which are 610GPa and 660 GPa, corresponding to the 23.0-nm-diameter and 21.5-nm-diameter SiC NRs. The agreement is good.

With orientation averages, the moduli of isotropic materials can be obtained. Two average methods, namely Reuss averages<sup>[56]</sup> ( $E_R$  and  $G_R$ ) and Voigt averages<sup>[57]</sup>, ( $E_V$  and  $G_V$ ) are adopted. According to the theory of Hill<sup>[58]</sup>, the physical averages, here denoted by subscript *a*, are the intermediate between the Reuss and Voigt averages. With these



considerations, Young' modulus and shear modulus of isotropic  $\beta$ -SiC are given as follows:

$$E_a \approx 448GPa \pm 2.2\%$$

$$G_a \approx 192GPa \pm 2.6\%$$

Compared with the previous first principle <sup>[37]</sup> and semi-empirical <sup>[38], [39]</sup> calculations, our results agree better with the experimental values. These results confirm the conclusion of Lambrecht: the random orientation hypothesis applies well to the ceramic samples. The average Possion ratio  $\nu_a$ , 0.17, is close to the experimental value. The small Possion ratio of  $\beta$  Si-C, as compared with other materials, *e.g.* Aluminum 0.347, demonstrates its high stiffness .

#### IV. LOADING ALONG DIRECTION [111]

In this loading direction, two loading modes are investigated: uniaxial extension and uniaxial tension. At the latter case, the transverse lattices contract in order to approach the energy minimum. With regard to the loss of symmetry of center inversion, the four Si-C bonds along directions [111],  $[1\bar{1}1]$ ,  $[11\bar{1}]$  and  $[\bar{1}11]$ , are not equivalent under [111] loading. The internal relaxation and lateral contraction must be considered. In our calculations, by using the lattice constant at room temperature, the internal relaxation is carried out after the transverse strains are obtained. The length of Si-C bond is 3.5673 (Bohr) under zero loading. As the loading is along [111] direction, the variation of bond length along the [111] direction will be more significant than that of the other three bonds. Fig.1 shows the energy, stress and force under uniaxial extension and uniaxial tension with or without internal displacement.(Without other statement, the strain, force and stress, given in figures, are the physical strain, applied force and Cauchy stress.) The corresponding transverse strain and internal displacement are given in Fig. 2 and Fig 3.

At the beginning of loading, as compared with the corresponding Si-C bond length without the internal relaxation, the difference among the four Si-C bond lengths is small, and no marked effect of relaxation and internal displacement through both the shuffle and glide

plane is shown. This phenomenon, shown in Fig.1, is obvious for  $\beta$ -SiC, a kind of high stiffness and low Poisson ratio covalent material. The strain energy curves of the three loading modes, *i.e.* uniaxial extension and uniaxial tension with or without internal relaxation are almost the same. Despite the fact that the stress and force of uniaxial tension is smaller than the uniaxial extension for the relaxation, they are still similar in these loading modes. Based on Kleinman's <sup>[59]</sup> discussion on Silicon with  $[111]$  strain, the internal strain tends to keep the bond length along the four unchanged unequivalent  $[111]$  directions. In our calculations, the internal displacement of atom along  $[111]$  direction, which is through the shuffle plane, is negative, and that of the remaining three Si-C bonds along the  $[\bar{1}\bar{1}1]$ ,  $[11\bar{1}]$  and  $[\bar{1}11]$  directions, through the glide plane, is positive. This means that the effect of relaxation always tends to diminish the difference of four Si-C bond lengths. With the increase of the longitudinal strain, the internal displacement through the shuffle plane becomes positive from negative, and that through the glide plane moves from positive to negative while approaching zero at the same point ( $e_z = 0.105$ ). The internal displacements for the two cases have the same magnitude but with the opposite sign. The details can be found in Fig.3. During the whole uniaxial tension, the magnitude of transverse strain increases monotonically.

With further increase of the longitudinal strain, the strain energy of uniaxial extension and of uniaxial tension without internal displacement still have approximately the same value. However, both the internal displacements through the shuffle plane and the glide plane change their signs (the symmetry is still hold). The uniaxial tension curve with internal relaxation softens quickly, and the shape of tensile curve changes dramatically. An energy plateau presents, and material becomes unstable. On the basis of the stress curve, the maximum stress of uniaxial tension with internal relaxation, namely the theoretical strength  $\sigma^{th}$ , is obtained and equal to 50.8 GPa. The corresponding critical macroscopic strain and internal displacement is 0.144 and 0.082 (Bohr), the Si-C bond length along  $[111]$  is 4.163 (Bohr). With the modified Tersoff potential, Tang and Yip <sup>[43]</sup> analyzed the brittle fracture of  $\beta$ -SiC under hydrostatic tension by molecular dynamics. They found that the mode of

instability of  $\beta$ -SiC was the spinodal instability, and the corresponding critical strain and pressure were 0.153 and 37.0 GPa. Therefore, both the first principle and empirical potential calculations gave a similar critical bond-length of  $\beta$ -SiC along [111].

Our result agrees well with the experimental value, given by Wong *et al.* <sup>[22]</sup>, 53.4 GPa, obtained for [111]-oriented SiC nanorod. This agreement also means that no other branching and instability modes exist during the uniaxial loading before it reaches the inflexion of energy-strain curve. It is worth while pointing out that the experimental strength measured is the bending strength. The tensile and bending strengths are comparable to  $\beta$ -SiC whisker <sup>[8], [15]</sup> and are also expected to be similar to  $\beta$ -SiC nanorod. <sup>[22]</sup> Petrovic *et al.* <sup>[15]</sup> measured the tensile strength of  $\beta$ -SiC whisker and their result is 23.74 GPa, which is far smaller than our theoretical calculation and Wong's experiment values for defects. Lambrecht *et al.* <sup>[37]</sup> calculated the tensile strength by Orowan expression with [111] surface energy, and the result is 30 GPa. With the similar formula, Op Het Veld and Veldkamp <sup>[60]</sup> obtained the theoretical cleavage strength 46.3 GPa, which is close to ours. The detailed comparison can be found in Table 2.

After  $e_z > 0.105$ , the internal displacement through the shuffle plane becomes positive, and that through the glide plane becomes negative. The distance between the atom through the shuffle plane along [111] increases, and that through the glide plane decreases, and a crack nucleates on the  $\{111\}$  shuffle plane. The internal displacements through the shuffle and glide plane at the critical strain are, respectively, 0.082 and -0.082. With further increase of the longitudinal strain, the internal displacements of the shuffle and glide planes also increase quickly. This positive and negative increase of internal displacements of shuffle and glide planes will result in a dramatic cleavage on the  $\{111\}$  shuffle plane and the mixing of Si and C atoms through the glide plane. The cleavage on  $\{111\}$  shuffle plane can be partly attributed to the lower surface energy than that of the  $\{111\}$  glide plane. <sup>[31], [43], [61]</sup> These results agree well with the previous molecular dynamics simulation. <sup>[43]</sup>

## V. BIAXIAL PROPORTIONAL EXTENSION

To consider only the biaxial proportional extension, this section deals with the extension along directions  $[010]$  and  $[001]$ , and not the internal atomic and volume relaxation. The strain ratio between  $[010]$  and  $[001]$  is 0.25, 0.5, 0.75 and 1. The results are shown in Fig.4. With the increase of the ratio, the energy, stress and maximum stress will increase at the same longitudinal strain accordingly. However, the critical strain is similar for different proportional loading modes.

## VI. LOADING ALONG DIRECTION $[001]$

In this section, we consider the uniaxial extension and uniaxial tension along direction  $[001]$ . The reference state is the state with the theoretical lattice constant. Symmetry of crystal under this loading mode is tetragonal. Unlike the loading along  $[111]$ , the deformation of the four Si-C bonds in this loading mode is the same and the four bonds are equivalent. There will not be any internal displacements and the internal relaxation can be neglected during the loading. We have made calculations at several strain with or without internal relaxation and found that the value of transverse strain at a specific longitudinal strain is the same. Our results are given in Fig.2, Fig.5

From Fig.5a, we can see that both of the strain energy for uniaxial extension and tension increase with the increase of the longitudinal strain. The strain energy of uniaxial extension is always larger than that of the uniaxial tension, as is expected. However, the energy difference between two loading modes is small, same as with the  $[111]$  loading. At a larger strain, the energy difference becomes even smaller. The applied force and stress of uniaxial tension are lower than those of the uniaxial extension for the triaxial stress state at the beginning and higher than them at the subsequent loading ( this phenomenon will be explained later). Just like Fig.5a, the difference of applied force and stress between these two loading modes is not significant.

In order to obtain the ideal strength and analyze the stability under uniaxial tension, we calculate the elastic constants and derive the stability criteria based on the stiffness coefficients. With the tetragonal symmetry, the number of independent elastic constants is reduced to six:  $C_{33}$ ,  $C_{12}$ ,  $C_{13} = C_{23}$ ,  $C_{11} = C_{22}$ ,  $C_{44} = C_{55}$  and  $C_{66}$ ; all the other  $C_{ij}$  are equal to zero. With equation 6, 7 and ??, we write the stability criteria as follows:

$$(C_{33} + \sigma)(C_{11} + C_{12}) - 2C_{13}(C_{13} - \sigma) \geq 0 \quad (12)$$

$$C_{11} - C_{12} \geq 0 \quad (13)$$

$$C_{44} + \frac{1}{2}\sigma \geq 0 \quad (14)$$

$$C_{66} \geq 0 \quad (15)$$

The first one involves the vanishing of bulk modulus, and is referred as spinodal instability. The second instability involves symmetry breaking (bifurcation) with the volume conservation; it may be identified as the tetragonal shear breaking and referred as Born instability. The third and fourth are two distinct shear deformation instabilities. Six strains are designed to calculate the independent elastic constants and given as follows:

$$e_{11} = e_{22} = \delta, e_{ij} = 0, i, j=1,2,3$$

$$e_{11} = -e_{22} = \delta, e_{ij} = 0, i, j=1,2,3$$

$$e_{11} = e_{33} = \delta, e_{ij} = 0, i, j=1,2,3$$

$$e_{11} = -e_{33} = \delta, e_{ij} = 0, i, j=1,2,3$$

$$e_{12} = e_{21} = \delta, e_{ij} = 0, i, j=1,2,3$$

$$e_{23} = e_{32} = \delta, e_{ij} = 0, i, j=1,2,3$$

In each case, the domain of strain is  $[0,0.02]$ . The results are shown in Fig.6

During uniaxial tension, the variation of mechanical properties on transverse section is comparatively small, and the corresponding elastic constants, *i.e.*,  $C_{11}$ ,  $C_{12}$ ,  $C_{66}$ , keep positive, as shown in Fig.6a. However, the elastic constants related to longitudinal strain change dramatically and even become negative at large strain, *e.g.*  $C_{13} \leq 0$  when  $e_{33} \geq 0.184$ ,

$C_{33} \leq 0$  when  $e_{33} \geq 0.352$ . Because  $C_{13} \leq 0$  leads to negative Possion ratio, the transverse section will expand with the increase of the longitudinal strain. This phenomenon is also shown in Fig.2, the transverse strain varies  $e_{11}$  proportionally with  $e_{33}$  when  $e_{33} \geq 0.20$ . Negative Possion ratio had also been investigated by Milstein *et al* [3], [4], [26], [62]. However, in their papers, negative Possion ratio only occurs at branching or unstable points, and the materials investigated are monatomic metal materials Fe and Ni. In the present calculations, it is surprising that  $\beta$ -SiC, a non-metal and two component crystal, is still stable at this negative Possion ratio, shown in Fig.6b. The same result is obtained when calculations with internal atomic relaxation are implemented. This phenomenon must be related with the bond nature of  $\beta$ -SiC. The charge transfer [63] and ionic component [64] of  $\beta$ -SiC will affect the mechanical response. The detailed analysis of electric structure should be carried out and further investigation is necessary. The lattice transverse expansion leads to much quicker increase of the force and stress of uniaxial tension than that of uniaxial extension and the values of the previous force and stress will be higher than those of uniaxial extension at a large strain.

On the basis of the stability criteria, we have found that the spinodal and Born instabilities are triggered almost at the same strain 0.37 with the transverse strain -0.0137. The corresponding strength, 101.3 GPa, which is almost twice of that for [111]- oriented SiC nanorod 53.4 GPa [22] for its smaller interplannar distance, is obtained. At this critical strain, the elongation strain along [111] direction is 0.129, comparable with the critical strain 0.144 under uniaxial lading along [111]. Tang and Yip [43] investigated the instability of  $\beta$ -SiC under hydrostatic tension with stiffness coefficient, and found that failure mode of  $\beta$ -SiC is spinodal instability. This was proved by their molecular dynamics simulations, and the nucleation of cracking on the {111} plane and decohesion were revealed. They also showed that a shear instability is triggered by the spinodal instability. All of these results are same with our first principle calculations.

## VII. SUMMARY AND CONCLUSION

On the basis of the DFT total energy calculation and stability theory, we give a detailed investigation of mechanical properties of two-atomic constituent materials  $\beta$ -SiC: energetics, elasticity, stress-strain relations, stability and strength under different loading modes and directions. The results are satisfactory.

Owing to the unequivalence of the four Si-C bonds under the uniaxial tension along  $[111]$ , the relaxation must be implemented and internal displacements be calculated. The internal displacements along the  $[111]$  direction and other three directions namely  $[\bar{1}11]$ ,  $[1\bar{1}1]$  and  $[11\bar{1}]$  have the same magnitude but the opposite sign. At the beginning of loading, the effect of relaxation is not significant and tends to diminish the difference of the four Si-C bond lengths. However, it becomes important at the subsequent loading and results in a crack nucleated on  $\{111\}$  shuffle plane, while the Si atom and C atom through the glide plane approach each other. The failure in this loading modes is of cleavage fracture. These conclusions are consistent with the previous molecular dynamics simulations. The theoretical strength obtained agrees well with the experimental data.

Under loading along  $[001]$ , the four Si-C bonds are equivalent for the tetragonal symmetry and the relaxation can be neglected. The strain energy, applied force and stress are similar despite two distinct loading modes, namely, uniaxial tension and extension. During the uniaxial loading along  $[001]$ , the spinodal and Born instabilities are triggered almost at the same strain. Previous molecular dynamics investigation revealed similar facts. Owing to the smaller interplanar distance, the corresponding ideal strength, 101 GPa, which is much higher than the theoretical strength for the loading along  $[111]$  and the experimental data, is obtained; however, the Si-C bond length for loading along  $[001]$  and  $[111]$  at the critical strain is close. There exists some stable range when the Poisson ratio is negative, and these phenomena are related to the unique bond nature of  $\beta$ -SiC, a kind of non-typical covalent material, which permits charge transfer. A detailed analysis of electronic structure will brought up for further investigation.

## ACKNOWLEDGMENTS

This work was supported by the National Natural Science Foundation of China (Grant No.19704100) and National Natural Science Foundation of the Chinese Academy of Sciences (Grant No. KJ951-1-201). One of authors W. X. Li wishes to thank Prof. D. S. Wang for his helpful discussion and encouragement. Parts of the computations are done at the super-parallel computer of the Network Information Center of the Chinese Academy of Sciences. We are also grateful to Prof. K. Wang for checking the manuscript.



## REFERENCES

- [1] J. Frenkel, Z. Phys., **37**, 572(1926).
- [2] A. Kelly, *Strong Solids*, 2nd ed. (Clarendon, Oxford,1973).
- [3] F. Milstein, Phys. Rev. B **3**, 1130(1971).
- [4] F. Milstein, I. Appl. Phys. **44**, 3833(1973).
- [5] F. Milstein, B. Farber, Phil. Mag. A **42**, 19(1980).
- [6] E. Esposito, A. E. Carlsson, D. D. Ling, H. Ehrenreich, C. D. Gelatt Jr., Phil. Mag. **41**, 251(1980).
- [7] A. T. Paxton, P. Gumbsch and M. Methfessel, Phil. Mag. Lett. **63** , 267(1991).
- [8] N. H. Macmillan, J. Mater. Sci. **7**, 239(1972).
- [9] M. Šob, L. G. Wang, V. Vitek, Mater. Sci. Engin. A **234 - 236** , 1078(1997); P. Šandera, J. Pokluda, L. G. Wang, M. Šob, *ibid*, A**234 - 236**, 370(1997).
- [10] F. Cleri, J. Wang, S. Yip, J. Appl. Phys. **77**, 1449 (1995).
- [11] J. Wang, S. Yip, S. Phillpot, and D. Wolf, Phys. Rev. Lett **77**, 4182(1993).
- [12] J. Wang, J. Li, S. Yip, S. Phillpot and D. Wolf, Phys. Rev. B **52** , 12627(1995).
- [13] K. Mizushima, S. Yip, E. Kaxiras, Phys. Rev. B **50**, 14952(1994).
- [14] R. L. Mehan and J. A. Herzog, in *Whisker Technology*, A. P. Levitt, Ed. (Wiley-Interscience, New York,1970), pp. 157-196.
- [15] J. J. Petrovic, J. V. Milewski, D. L. Rohr, F. D. Gac, J. Mater. Sci. **20**, 1167(1985); J. J. Petrovic and R. C. Hoover, *ibid*. **22**, 517(1987); N. H. Macmillan, *ibid*. **7**, 239(1972).
- [16] T. W. Ebbesen and P. M. Ajayan, Nature **358**, 220(1995).
- [17] D. T. Colbert *et al.*, Science **266**, 1218(1994).

- [18] T. Guo, P. Nikolaev, A. Thess, D. T. Colbert, R. E. Smalley, Chem. Phys. Lett. **243**, 49(1995); A. Thess *et al.*, Science **273**, 483(1996).
- [19] H. Dai, E. W. Wong, Y. Z. Lu, S. Fan, C. M. Lieber, Nature **375**, 769(1995).
- [20] P. Yang, C. M. Lieber, Science **273**, 1836(1996).
- [21] H. Dai, E. W. Wong, C. M. Lieber, Science, **272**, 523(1996).
- [22] E. W. Wong, P. E. Sheehan, C. M. Lieber, Science **277**, 1971(1997).
- [23] M. Polanyi, Z. Phys. **7**, 323(1921).
- [24] E. Orowan, Z. Krist. A **89**, 327(1934); *Idem*, Reports Prog. Phys. **12**, 185(1949); *Idem*, Weld. J. **34**, 157(1955).
- [25] F. Milstein, J. Mater. Sci **15**, 1071(1980).
- [26] F. Milstein, K. Huang, Phys. Rev. B, **18**, 2529(1978).
- [27] F. Milstein, R. Hill, K. Huang, Phys. Rev. B **21**, 4282(1980).
- [28] F. Milstein, B. Farber, Phys. Rev. Lett. **44**, 277(1980).
- [29] P. Hohenberg, and W. Kohn, Phys. Rev. **136**, B864(1964); W. Kohn and L. J. Sham, *ibid* **140**, A1133(1965)
- [30] M. Born, Proc. Cambridge Phil. Soc. **36**, 160(1940); M. Born and K. Huang, *Dynamical Theory of Crystal Lattices* (Clarendon, Oxford, 1956).
- [31] R. Hill, Math. Proc. Cambridge Philos Soc. **77**, 225(1975).
- [32] R. Hill, F. Milstein, Phys. Rev. B **15**, 3087(1977).
- [33] F. Milstein and R. Hill, Phys. Rev. Lett. **43**, 1411(1979); *Idem* J. Mech. Phys. Solids **25**, 457(1977); *Idem ibid* **26**, 213(1978); F. Milstein, in *Mechanics of Solids*, edited by H. K. Hopkins and M. J. Sewell(Pergamon, Oxford, 1982), p. 417.

- [34] W. X. Li and T. C. Wang, J. of Phys: Condens Matter **10**, 9889(1998).
- [35] N. Churcher, K. Kunc, and V. Heine, J. Phys. C **19**, 4413(1986).
- [36] (a). C. Cheng, R. J. Needs and V. Heine, J. Phys. C **21**, 1049(1988); (b). J. J. A. Shaw and V. Heine, J. Phys. Condens. Matter **2**, 4351(1990) (c). C. Cheng, V. Heine and L. Jones, *ibid.* **2**, 5097(1990); (d). C. Cheng, V. Heine and R. J. Needs, *ibid* **2**, 5115(1990).
- [37] W. R. L. Lambrecht, B. Segall, M. Methfessel and M. van. Schilfgaarde Phys. Rev. B **44**, 3685(1991).
- [38] K. B. Tolpygo, Fiz. Tverd. Tela(Leningard) **2** 2655(1960) [Sov. Phys.- Solid State **2**, 2367(1961)].
- [39] J. Teroff, Phys. Rev. B **39**, 5566(1989).
- [40] E. Pearson, T. Takai, T. Halicioglu, and W. A. Tiller, J. Cryst. Growth **70**, 33(1984).
- [41] M. Kohyama, S. Kose, M. Kinoshita, and R. Yamamoto, J. Phys. Condensed Matter **2**, 7791(1990).
- [42] J. A. Majewski and P. Vogl, Phys. Rev. B **35**, 9666(1987).
- [43] M. Tang, S. Yip, J. App. Phys. **76**, 2719(1994).
- [44] C. Truesdell and R. Toupin, *Handbuch der Physik*, edited by S. Flügge (Springer-Verlag, Berlin, 1960), Vol. III/1, p. 226.
- [45] M. Bockstedte, A. Kley, J. Neugebauer and M. Scheffler, Comput. Phys. Commun. **107**, 187(1997).
- [46] D. R. Hamman, Phys. Rev. B **40**, 2980(1989).
- [47] N. Troullier, J. L. Martins, Phys. Rev. B **43**, 1993(1991).
- [48] M. Fuchs, M. Scheffler, Comput. Phys. Commun., to be published

- [49] X. Gonze, R. Stumpf, M. Scheffler, Phys. Rev. B **44**, 8503(1991).
- [50] J. Perdew, A. Zunger, Phys. Rev. B **23**, 5048(1981).
- [51] C. S. G. Cousins, J. Phys. C: Solid St. Phys. **11**, 4867(1978); *ibid*, 4881(1978).
- [52] J. F. Nye, *Physical Properties of Crystals* (Clarendon, Oxford, 1957), Chap. VIII.
- [53] *Landolt Börnstein: Numerical Data and Functional Relationships in Science and Technology*, edited by O. Madalung, New Series, Group III, Vol. **17a** (Springer, Berlin, 1982), p, 49.
- [54] R. D. Carnahan, J. Am. Ceram Soc. **51**, 223(1968).
- [55] D. W. Feldman, J. H. Parker, Jr., J. W. Choyke, and L. Patrick, Phys. Rev. B **173**, 787(1968).
- [56] A. Reuss, Z. Angew, Math. Mech. **9**, 55(1929).
- [57] W. Voigt, *Lehrbuch de Kristalphysik* (Teubner Leipzig, 1928).
- [58] R. Hill, Proc. Phys. Soc. London Sect. A **65**, 349(1952).
- [59] L. Kleinman, Phys. Rev. **128**, 2614(1962).
- [60] A. J. G. Op Het Veld and J. D. B. Veldkamp, Fibre Sic. Technol. **2**, 269(1970).
- [61] B.N. Oshcherin, Phys. Status Solidi A **34**, K181(1976).
- [62] F. Milstein, K. Huang, Phys. Rev. B **19**, 2030(1979).
- [63] W.A. Harrison, *Electronic structure and the Properties of Solids* (Cambridge University Press, New York, 1975), p. 17.
- [64] A. R. Verma and P. Krishna, *Polymorphism and Polytypism in Crystals*, (Wiley, New York, 1966), p. 103.

# TABLES

TABLE I. Equilibrium and elastic modulus of  $\beta$ -SiC. PP-PW, present pseudopotential plane wave calculations; FP-LMTO, Lambrecht (Ref.26); CKH, Churcher, Kunc and Heine (Ref.24); Tolpygo (Ref. 22); Tersoff (Ref.23); Exp., experimental values as indicated by footnotes. The length unit is bohr radius, and modulus is GPa, the anisotropy  $A=2C_{44}/(C_{11} - C_{12})$ .

	PP-PW	FP-LMTO	CKH	Tolpygo	Tersoff	Exp.
$a_0$	8.166	8.154	8.145		8.164	8.238 <sup>a</sup>
$B_0$	225	223	224	211	220	225 <sup>b</sup>
$C_{11}$	405	420		352.3	420	390 <sup>c</sup>
$C_{12}$	135	126		140	120	142 <sup>c</sup>
$C_{44}$	254(270)	287		232	260	256 <sup>c</sup>
A	1.88	1.95		2.20	1.73	2.00 <sup>c</sup>
$E_{111}$	558	603		511	560	581( $\pm 10\%$ ) <sup>d</sup> 610 <sup>e</sup>
$E_{100}$	338	362		272	367	
$E_R$	441	476		378	462	
$E_V$	474	516		424	488	
$E_a$	458	496		401	475	448 <sup>b</sup>
$G_R$	188	208		157	201	
$G_V$	206	231		182	216	
$G_a$	197	219		169	208.5	192 <sup>b</sup>
$\nu_a$	0.173	0.146		0.201	0.150	0.168 <sup>b</sup>

<sup>a</sup> Landolt and Börnstein( [53])    <sup>b</sup> Carnahan( [54])    <sup>c</sup> Obtained from sound velocities ( [55])

<sup>d</sup> Experimental values from whisker( [15])    <sup>e</sup> Experimental values from nanorods( [22])

TABLE II. The Young's modulus and strength compared to other theoretical calculations and experiments; Here, ts, bs and cs means the tensile strength, the bending strength and the cleavage strength. The unit is GPa.

	$E$	$\sigma_{ts}$	$E^a$	$\sigma_{ts}^a$	$\sigma_{cs}^b$	$E^c$	$\sigma_{bs}^c$	$E^d$	$\sigma_{ts}^d$
[111]	558	50.4(0.144)	603	30	46.3	610	53.4	580 $\pm$ 10%	23.74
[001]	338	101(0.37)	362						

<sup>a</sup> From FP-LMTO and Orwan expression citelambrecht    <sup>b</sup> From Orwan expression [60]

<sup>c</sup> Experimental values from nanorods [22]    <sup>d</sup> Experimental values from whiskers [15]

## FIGURES

FIG. 1. (a) The calculated strain energy under the uniaxial extension and uniaxial tension with or without internal relaxation; (b) Applied force and stress under uniaxial tension with or without relaxation.

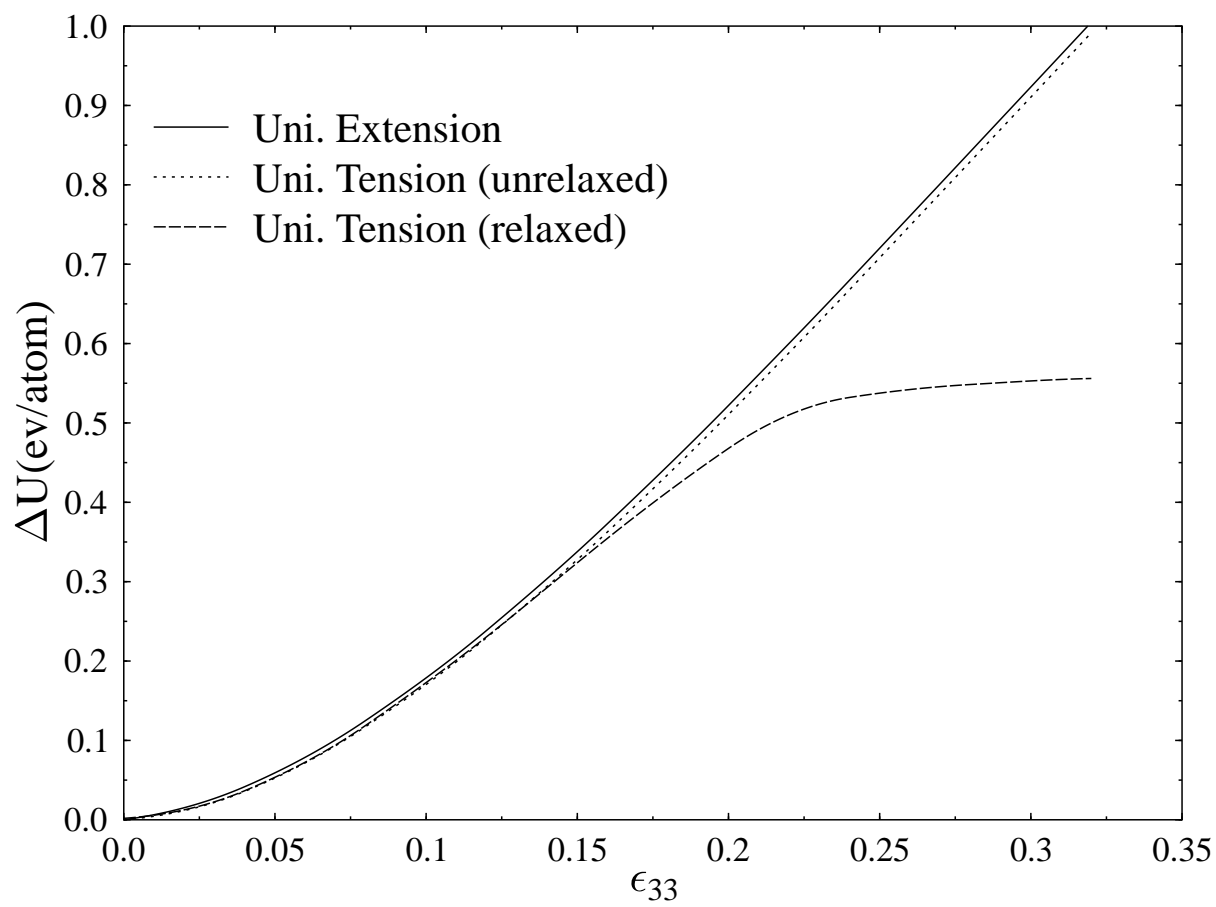
FIG. 2. The transverse strain of uniaxial tension along directions  $[001]$  and  $[111]$ .

FIG. 3. The internal displacement through shuffle and glide plane under  $[111]$  uniaxial tension. The club is for the shuffle plane, and the square is for the glide plane.

FIG. 4. The calculated strain energy(a) and applied stress(b) during biaxial proportional extension with difference ratio along  $[010](e_{22})$  and  $[001](e_{33})$  direction.

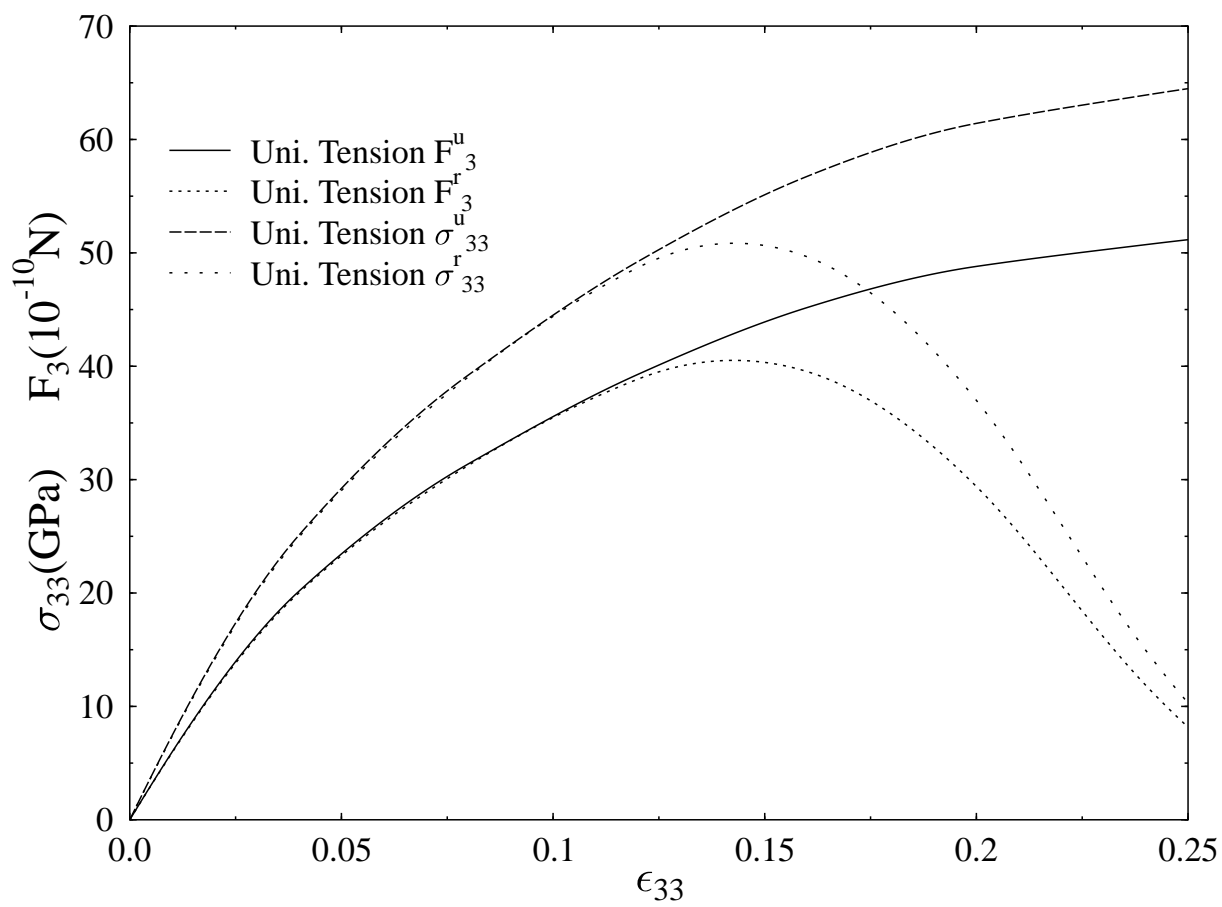
FIG. 5. The calculated strain energy (a), applied force and stress (b) of uniaxial extension and uniaxial tension along direction  $[001]$ .

FIG. 6. The calculated elastic constants (a) and stability (b) during uniaxial tension along direction  $[001]$ .

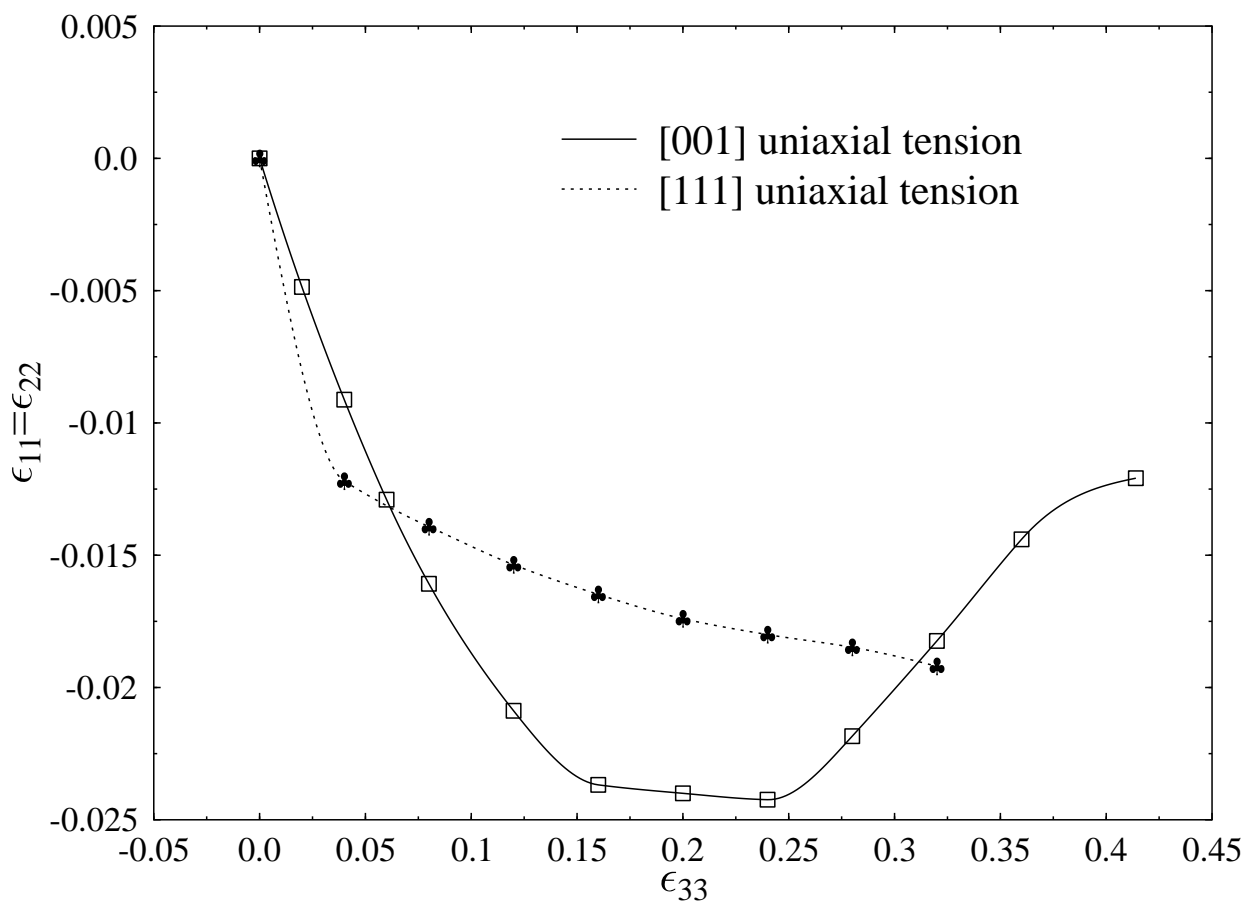


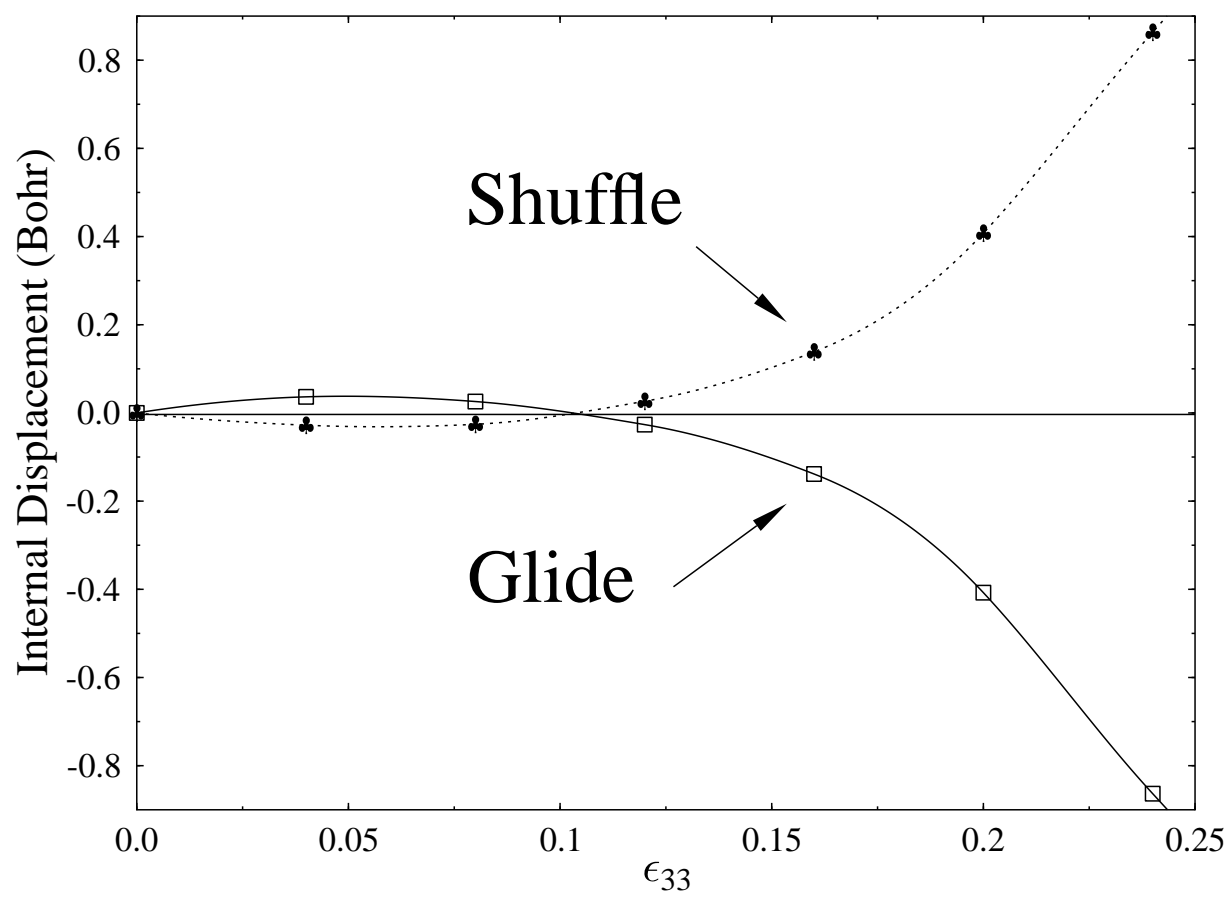
(a)

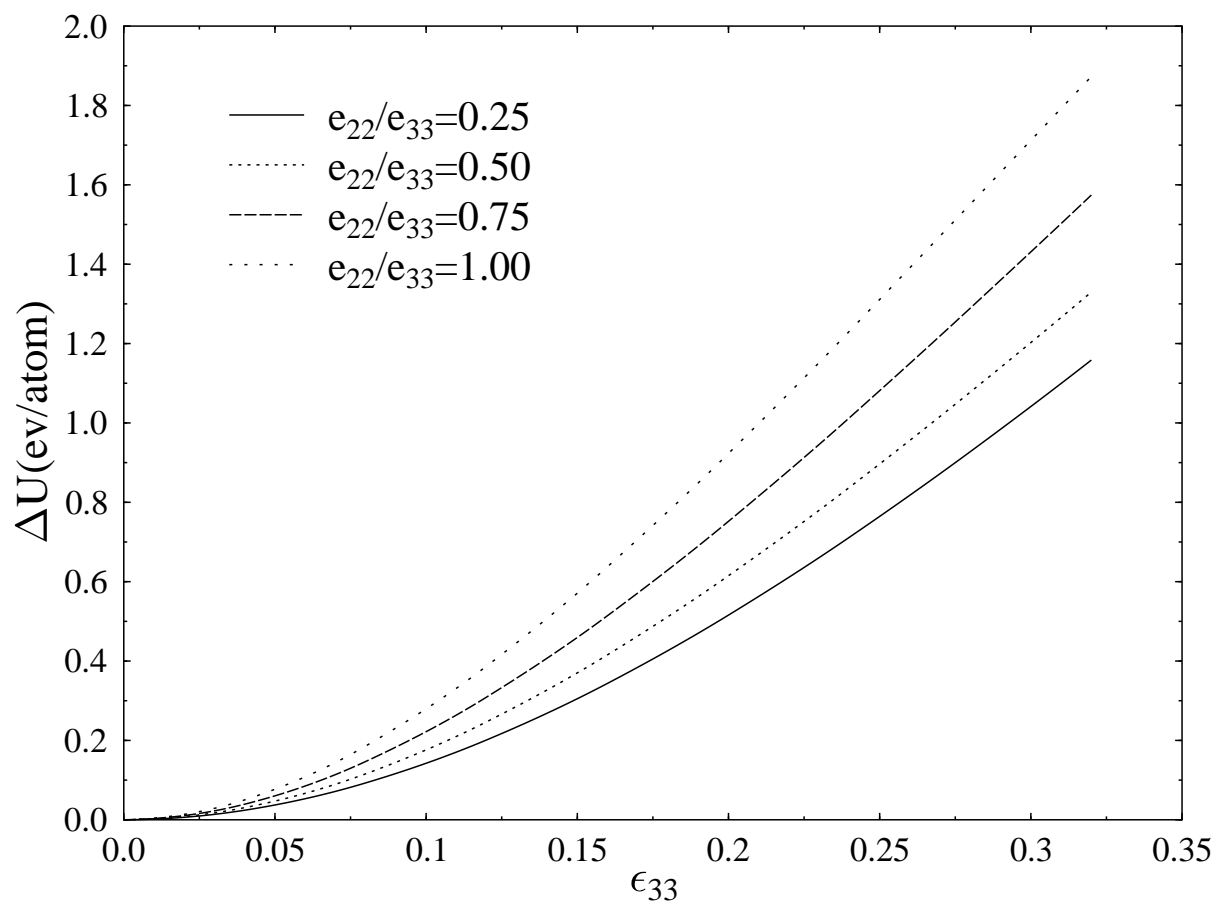




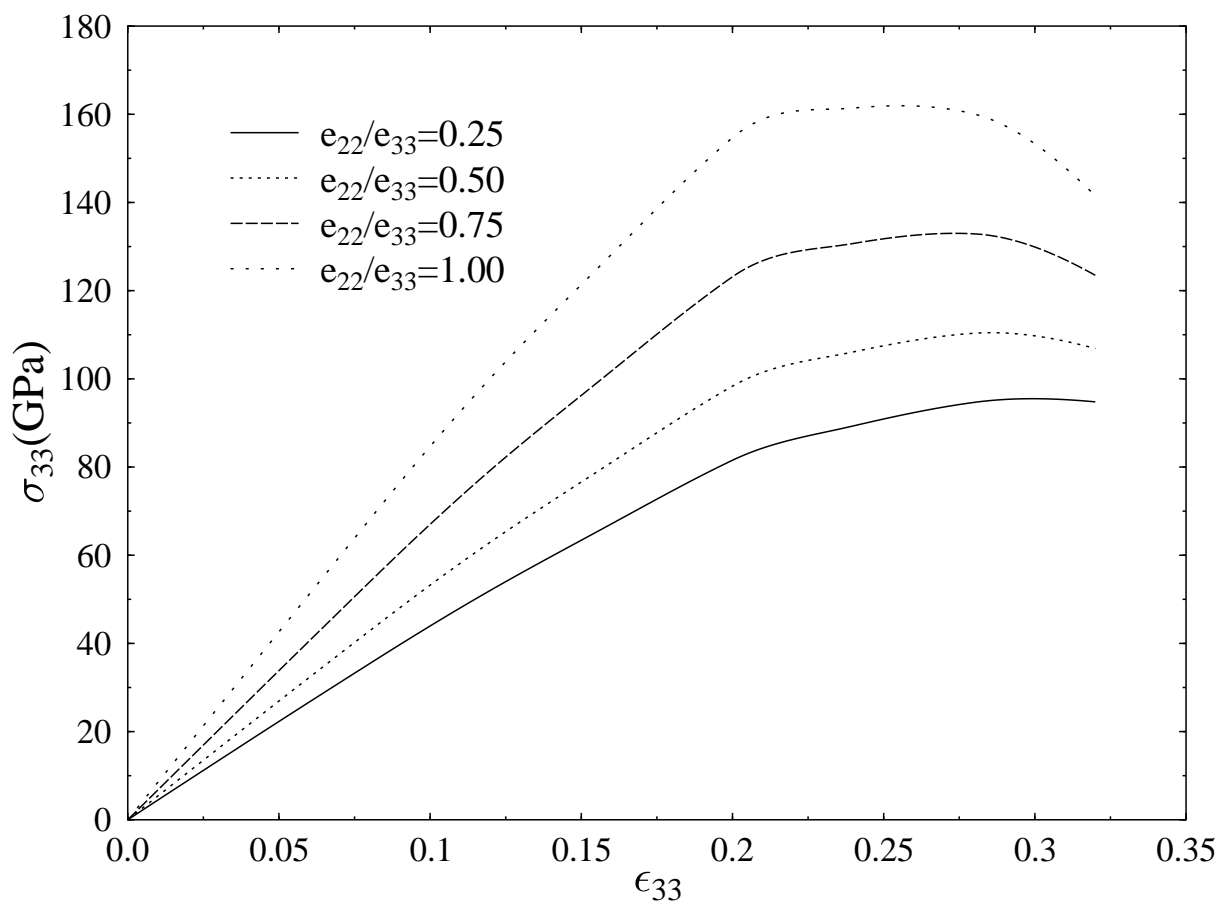
(b)



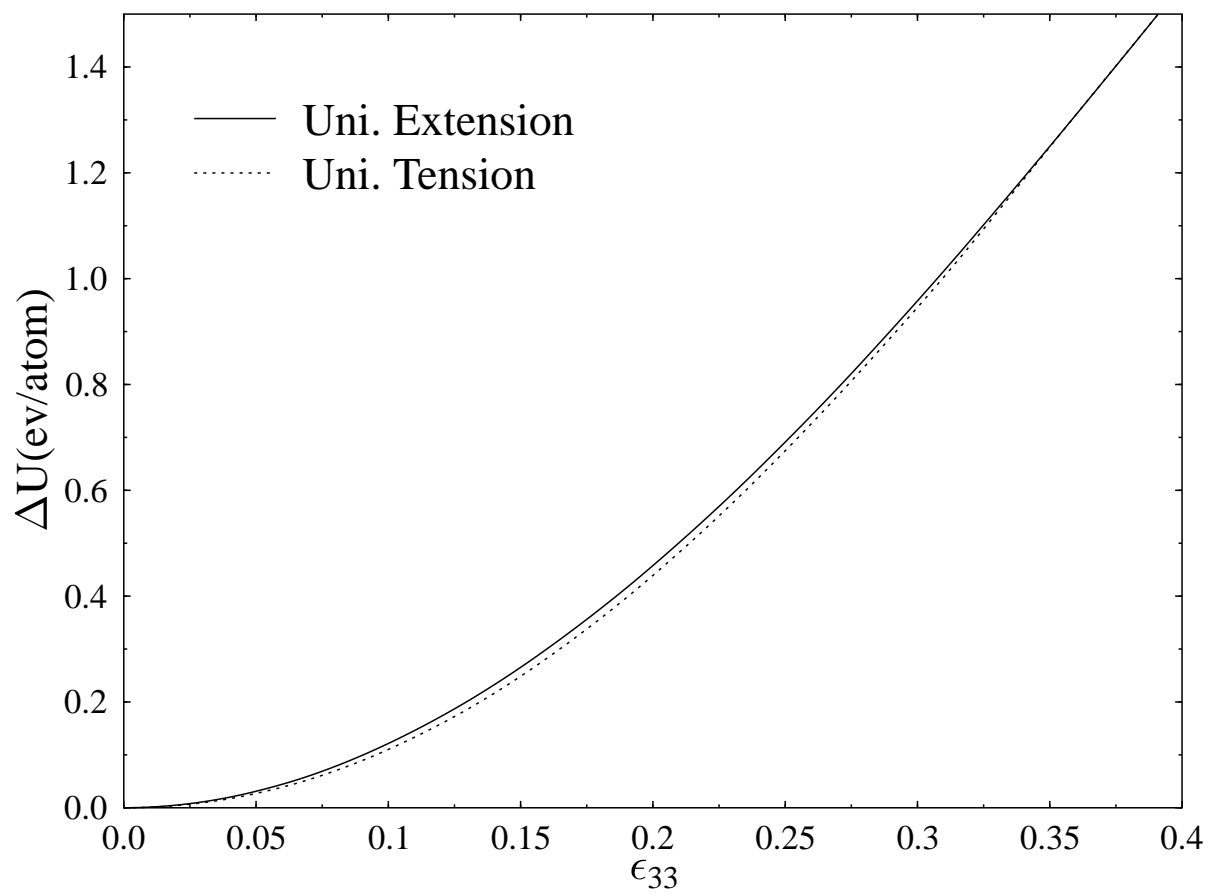




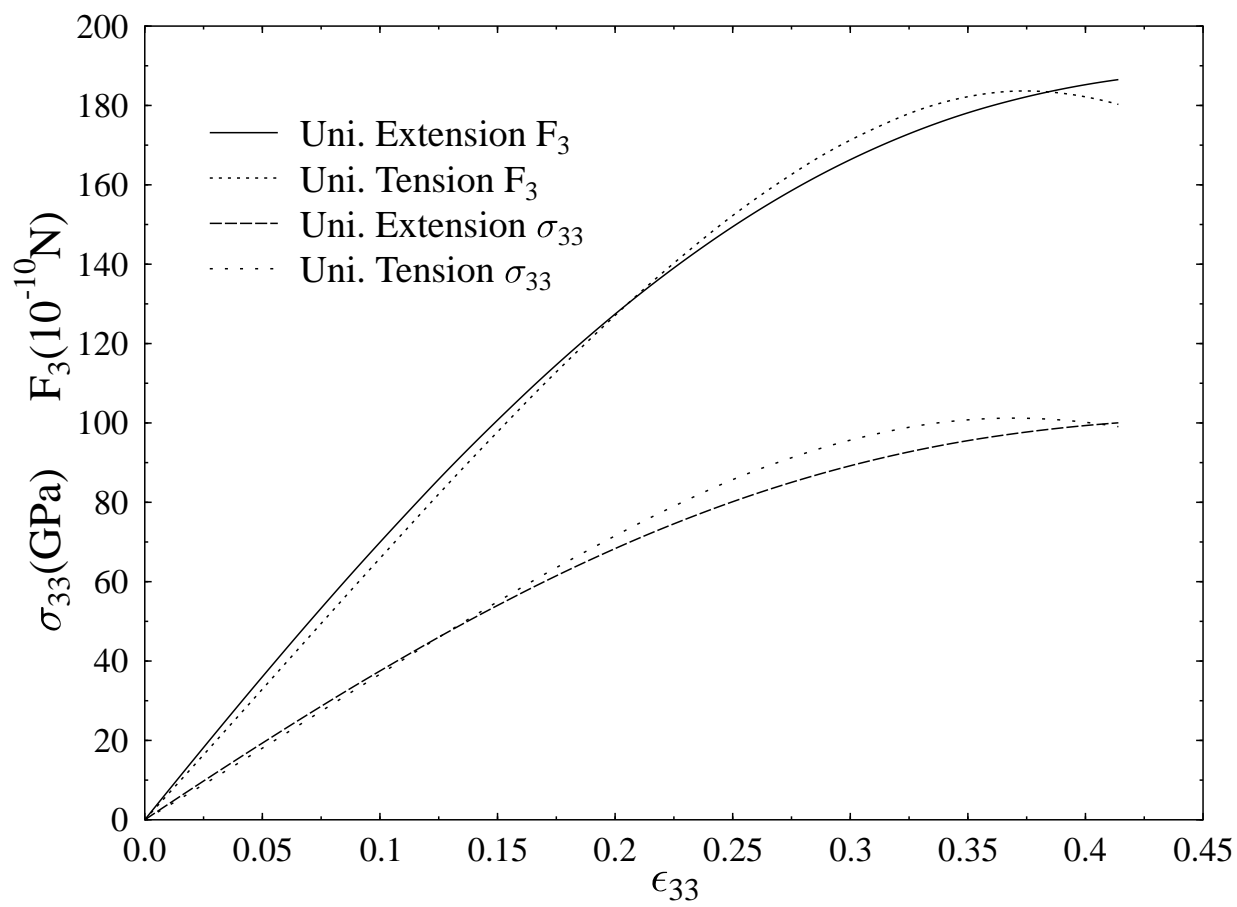
(a)



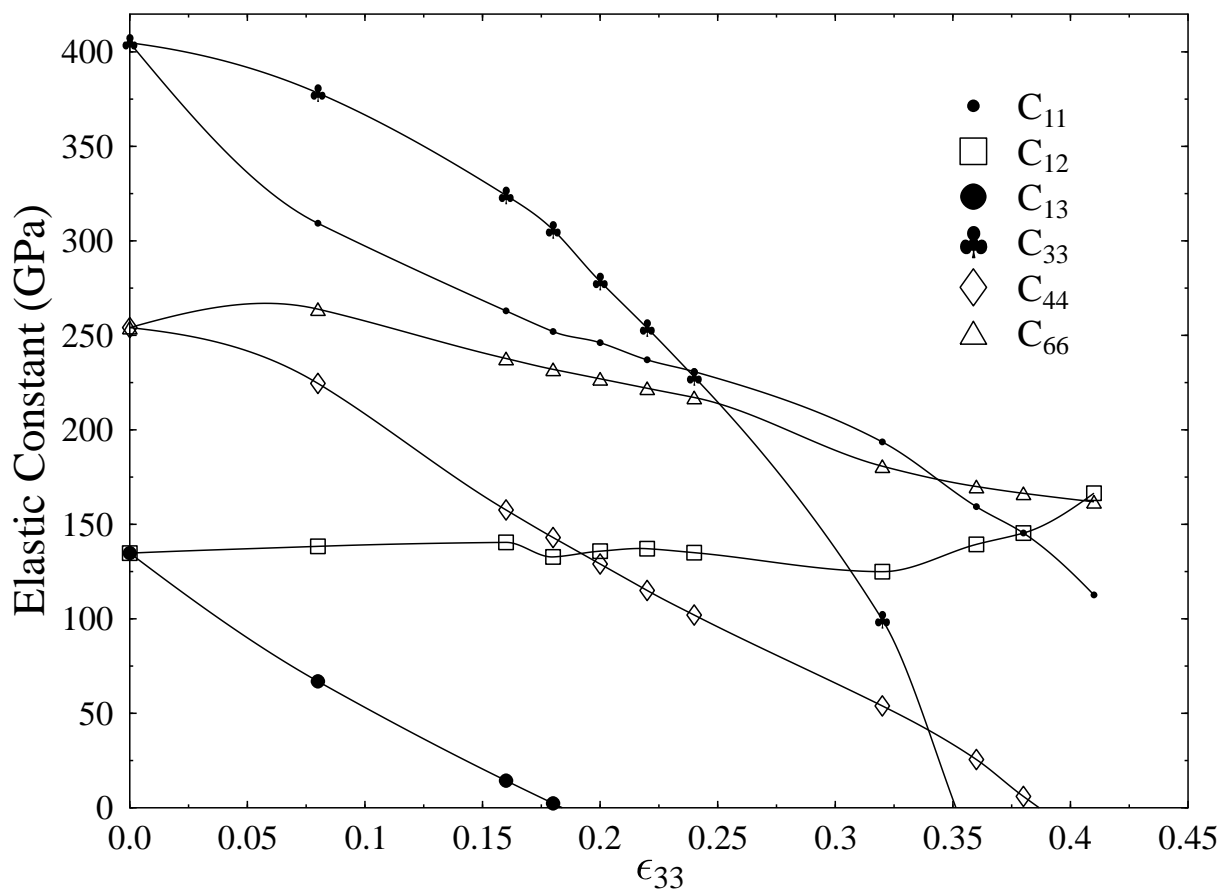
(b)



(a)

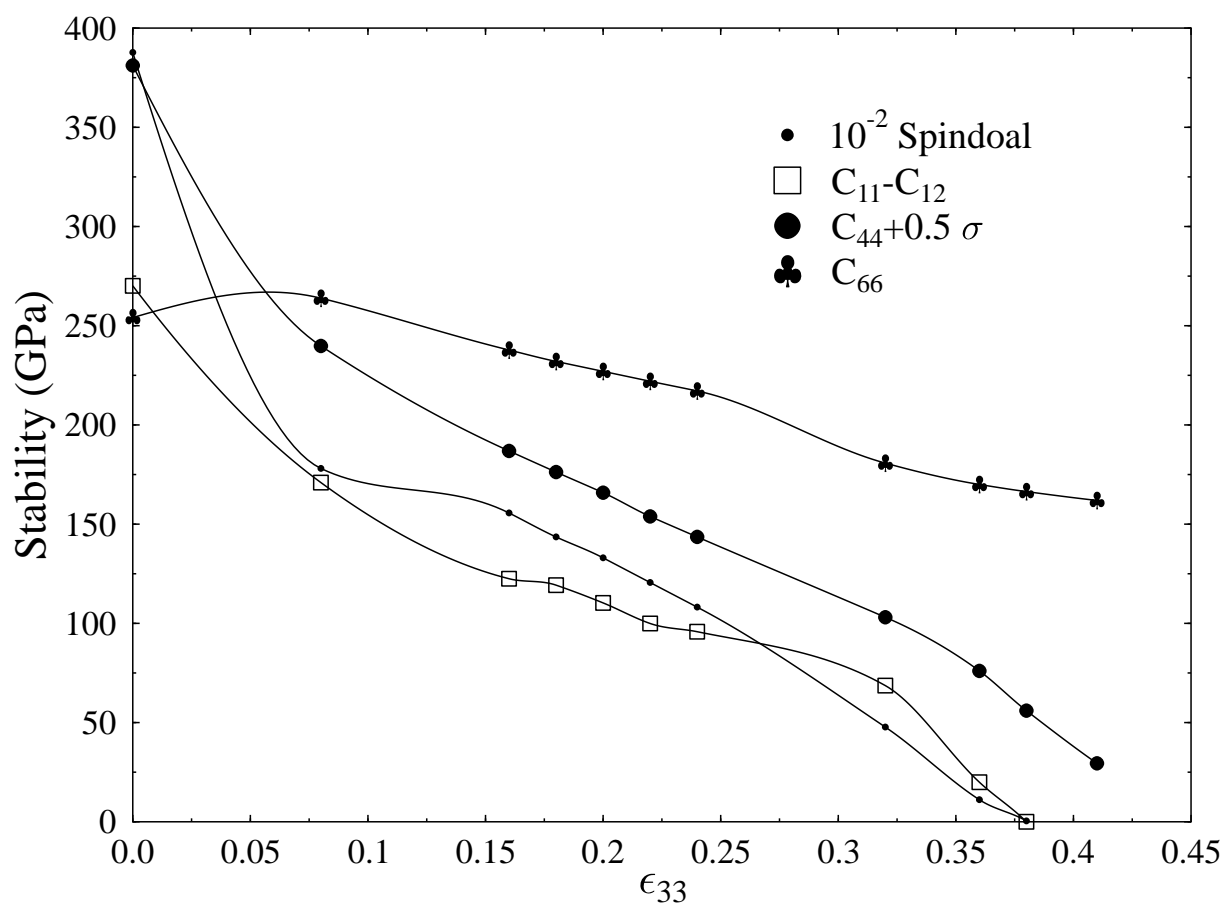


(b)



(a)





(b)